Drag Force Simulation on Blast Loaded Fabric Roof

Michalis Hadjioannou, Eric Sammarco, Matt Barsotti

Protection Engineering Consultants LLC, Austin, TX, USA

1 Abstract

An important consideration in predicting the dynamic motion of highly deformable structures subject to blast loads is the effect of drag force. A representative example of this condition is a blast-loaded non-breathable fabric roof, typically used for tents or other aesthetic fabric structures. A fully coupled fluid-structure interaction (FSI) analysis to simulate the interaction of the fabric roof with the air domain is theoretically possible, but is complex and requires significant computational effort. This study presents an alternative approach of including drag force in LS-DYNA® without the need to employ any form of computational fluid dynamics (CFD). Using the keyword ***LOAD_MOTION_NODE**, the velocity component of each node of the roof fabric elements is used as a variable to calculate the nodal drag force using the dynamic pressure equation. The calculated drag force is then applied at each time step as a nodal force that is opposite to the direction of motion and parallel to the element normals that represent the roof fabric. Results from a validation study using this approach are presented, and a case study involving the response of an arched roof fabric canopy subjected to blast loads is also discussed.

2 Introduction

2.1 Lightweight Fabric Structures

Lightweight fabric structures are a common type of structure used to enclose or to provide coverage over relatively large areas. The supporting structure usually consists of a steel frame where the fabric is attached. In the case of basic roof canopies, the fabric is laying over the supporting frame; in more advanced, aesthetically pleasing structures, the fabric is tensioned against the supporting frame. An example of a simple fabric shelter is shown in Fig. 1(a) and a tensile fabric structure that provides coverage over the stands of a stadium is shown in Fig. 1(b).

(a) Fabric shelter (non-tensioned) [1]

(b) Tensile fabric canopy, Don-Valley-Stadium [2]

Fig.1: Examples of lightweight fabric structures

2.2 Problem Statement

Because of the fabric's low self-weight, the need for intermediate supports is sparse which makes them more attractive over conventional structural types such as reinforced concrete (RC) or steel structures. However, the low mass of the fabric combined with its flexibility and tendency to resist load mainly through tensile membrane action, results in relatively high deformations under extreme loading conditions. A representative example of such loading condition is blast. While a well-designed RC roof may deform a few centimeters in response to a blast load, a fabric roof is expected to deform a few meters in response to blast. Due to the impulsive nature of the blast load, the fabric will move into space a few meters at a relatively high velocity. The dynamic motion of the fabric in space will generate an

appreciable amount of drag force that will act as attenuating force to the fabric's blast-induced motion. Therefore, to accurately predict the response of the fabric under blast loads, the drag force should be included in the calculation.

A fully coupled FSI analysis to simulate the dynamic motion of the fabric within the air domain is possible, but it is complex and requires significant computational effort. In design practice, performing FSI analysis to evaluate the response of a lightweight fabric structure to blast can be cumbersome and cost-prohibitive. This study presents an alternative approach to simulate the dynamic motion of the fabric in space that is aligned with code-based design approaches. This alternative is reasonably accurate, as the dynamic drag force of a moving object is calculated as a function of its transient (instant) velocity.

2.3 Fluid Structure Interaction Approaches

Previous efforts to simulate the dynamic motion of an object in a fluid are based on CFD models coupled with Lagrangian mesh descriptions. A common approach used in LS-DYNA is the Arbitrary Lagrangian-Eulerian (ALE) method to simulate the fluid and Lagrangian 4-node shell elements or 8-node solid elements for the moving object. Coupling with the moving object is employed with the ***CONSTRAINED_LARGANGE_IN_SOLID** keyword. Examples of this methodology have been used to simulate parachutes [3], [4] and water impact of a hemisphere [5]. For highly complex FSI problems, the incompressible flow (ICFD) solver of LS-DYNA coupled to Lagrangian mesh models has been employed [6]. These approaches, when properly used, have been shown to successfully simulate the FSI behavior of a solid object in a fluid. Their validation with benchmark problems and physical tests demonstrated their accuracy. However, they require significant computational overhead, which, for larger models, is sometimes impractical.

A simplified and computationally efficient FSI approach was used by Laird [7] to simulate the interaction of subsea lifting ropes with ocean currents. The effects of fluid drag forces and vortex shedding on the ropes were implicitly included in the analysis using simple drag force equations in lieu of modelling the fluid domain. A user loading subroutine applied drag and vortex shedding induced forces as nodal loads over the length of the cable as a function of the sea current velocities. The approach presented in this work for blast-induced drag force lies on the same basis but does not require usage of a user subroutine. Rather, standard LS-DYNA keywords are used to include the effects of dynamic drag force to the motion of an object in air.

3 Description of Proposed Methodology

The proposed methodology uses transient nodal velocities of the exposed surface elements of a moving object to calculate the pressure induced nodal surface forces at the vicinity of each node due to its motion inside a fluid. The nodal velocity, V_i, of the i_{th} node generates dynamic pressure, $p_{d,i}$, due to its motion inside a fluid with density, ρ_f. The dynamic pressure, $p_{d,i}$, is given by the following equation:

$$p_{d,i} = \frac{1}{2}\rho_f V_i^2 \tag{1}$$

The resulting dynamic pressure, $p_{d,i}$, is then multiplied by the tributary area, A_i, of the i_{th} node based on the size of the conjugate element yielding the nodal surface force, $F_{d,i}$:

$$F_{d,i} = p_{d,i} A_i \tag{2}$$

The magnitude of the nodal force, $F_{d,i}$, is entirely accurate at the stagnation point (Fig. 2) where the pressure coefficient, C_p, is equal to unity [8]. Depending on the shape of the moving body, the pressure distribution and thus the pressure coefficient, C_p, around its exposed surface varies. Therefore, the surface nodal forces are more accurately defined by the following equation:

$$F_{d,i} = p_{d,i} A_i C_p \tag{3}$$

An example of the variation of the pressure coefficient, C_p, around a circular body is shown in Fig. 2. The direction of the resulting nodal surface forces, $F_{d,i}$, is always parallel to the surface normals of the conjugate element with which each node is associated.

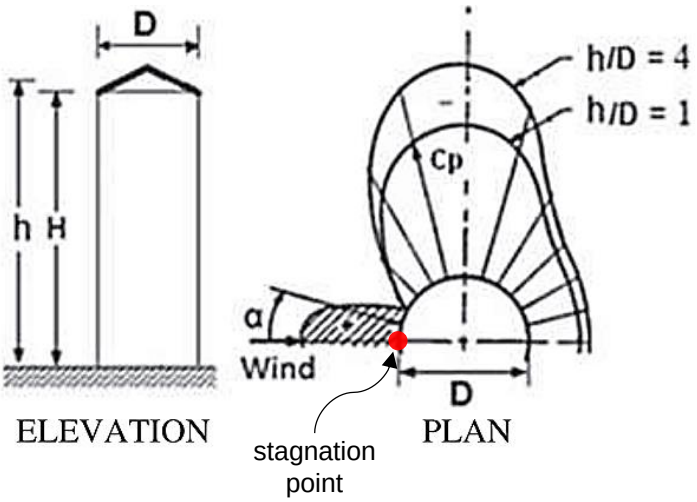

Fig.2: Stagnation point and pressure distribution around a circular body [9]

3.1 Limitations

Due to the single time-varying input parameter (V_i), this methodology is inherently limited to a constant pressure coefficient C_p and thus cannot represent the variation of pressure distribution around the exterior surface of a moving object due to physical phenomena such as fluid separation and skin friction [8]. Consequently, the proposed methodology is accurate for objects with an approximately uniform pressure distribution due to their motion in a fluid, such as planar or nearly planar surfaces. For planar shapes, the pressure coefficient, C_p, can be substituted by the drag coefficient, C_d, which, for Reynolds number above 1,000, varies between unity and two depending on the aspect ratio of the plate [10]. With this approach, the drag force due to the plate's motion inside the fluid domain can be captured with accuracy.

Adversely, for closed bodies such as cylinders (Fig. 2), spheres and random geometric shapes, pressure gradients on exposed surface(s) cannot be captured. Nonetheless, if the drag coefficient, C_d, of the body is known, then a pseudo-pressure coefficient, $C_{p,s}$, can be calculated. $C_{p,s}$ should be defined such that multiplying by the resultant of the surface nodal forces $\sum F_{d,i}$ parallel to the direction of motion will result in the theoretically calculated drag force. For a known moving velocity, V, drag force is equal to the velocity pressure multiplied by the projected area of the object, A_p, and by the drag coefficient, C_d. Therefore, $C_{p,s}$ is expressed by the following equation:

$$C_{p,s} = \frac{\frac{1}{2}\rho_f V^2 A_p C_d}{\sum F_{d,i}} \tag{4}$$

In this case, the surface nodal forces will be correct "on average" and drag force will be accurately included in the analysis. Despite these limitations, the proposed methodology is adequately accurate for design-level analyses where the focus is structure-level response that accounts for the effects of drag force. More importantly, as the object moves inside the fluid domain, the drag force varies as a function of its velocity.

3.2 Implementation in LS-DYNA

This methodology, as described above, can implemented in LS-DYNA with a combination of the following keywords:

- **`*DEFINE_COORDINATE_NODES`**, FLAG=1
- **`*LOAD_MOTION_NODE`**
- **`*DEFINE_FUNCTION`**

First, individual local coordinate systems are defined for all elements on the exterior surface of the moving object using **`*DEFINE_COORDINATE_NODES`** keyword. The coordinate system is updated at each time step by setting FLAG=1. This is a necessary setting, especially when large deformations are

expected. The total number of local coordinate systems should be equal to the number of exterior elements. Then, for each node that is associated with each one of these elements, a feedback loop is created using ***LOAD_MOTION_NODE**. This loop provides the nodal velocity of that node (NODE2) at each time step, calculates the corresponding nodal surface force, $F_{d,i}$, with ***DEFINE_FUNCTION**, and applies the resulting nodal force at this node (NODE1=NODE2). The input nodal velocity is chosen as the velocity component normal to the surface of the conjugate element with appropriate association of the local axes of each element with the defined degrees of freedom (DOF) in ***LOAD_MOTION_NODE**. Likewise, the resulting nodal force is also normal to the surface of the conjugate element so that it obeys the governing fluid mechanics principles (fluid pressure is always normal to a surface). The direction of the resulting nodal force is always applied opposite to the direction of motion of that node. The total number of feedback loops (number of ***LOAD_MOTION_NODE** keywords) should be equal to the number of specified local coordinate systems multiplied by the nodes of each element, i.e. multiplied by four for 4-noded shell elements. It is convenient to have a model with the same element size so that the tributary area, A_i, for the calculation of nodal force remains constant. Otherwise, same-size elements must be grouped and the velocity-induced nodal loads will be calculated with different ***DEFINE_FUNCTION** keywords for each element group.

4 Validation

Three models were analyzed using the proposed approach to validate the correct application of drag forces with LS-DYNA. The first two models involved a rigid sphere and a rigid square plate under gravitational acceleration. The third model involved a flat fabric piece with a suspended concentrated mass.

4.1 Terminal Velocity of Rigid Objects

The first two simulations involved two rigid objects in free fall. The theoretical value of the terminal velocity (V_t) of each object at free fall in the air ($\rho_{air} = 1.225\ kg/m^3$) was theoretically calculated with the following equation:

$$V_t = \sqrt{\frac{2mg}{\rho_{air} A_p C_d}} \tag{5}$$

where, m, object mass, g, gravity acceleration, A_p, projected area, C_d, drag coefficient.

The properties and theoretical terminal velocity of the sphere (Fig. 3) are summarized in Table 1. Fig. 4 shows the velocity history from the LS-DYNA simulation and the corresponding resultant force acting on the sphere. The sphere accelerates until the gravity forces equilibrate the drag force. After this point, the sphere reaches its theoretical terminal velocity and the resultant force drops to zero once the gravity force, i.e. weight, reaches equilibrium with the drag force. Similar behavior can be observed for the square rigid plate shown in Fig. 5 with properties summarized in Table 2. The response of the free fall simulation of the square plate is shown in Fig. 6.

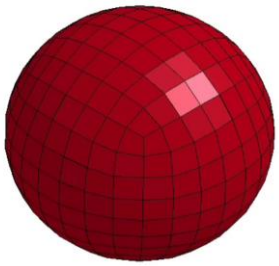

Fig.3: Rigid sphere FEM model

Diameter	0.5	m
Mass	5.0	kg
Gravity acceleration	9.8	m/sec^2
Weight	49.0	N
Projected area	0.2	m^2
Drag coefficient	0.5	
Terminal velocity	28.6	m/sec

Table 1: Rigid sphere properties

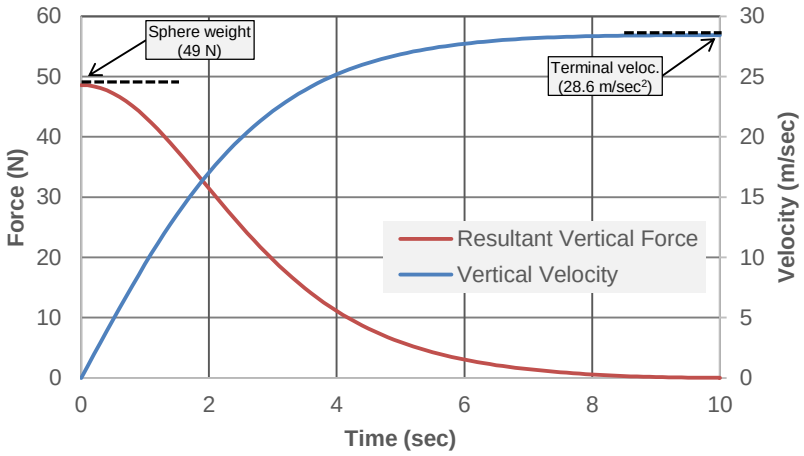

Fig.4: Velocity and resultant force history plot of sphere

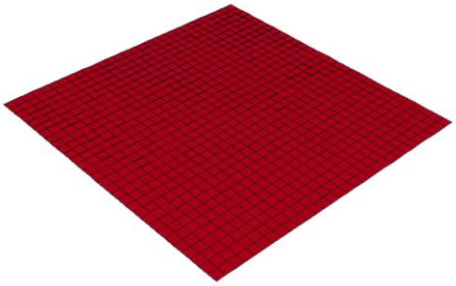

Fig.5: Rigid square plate FEM model

Edge length	1.5	m
Mass	100.0	kg
Gravity acceleration	9.8	m/sec^2
Weight	980.6	N
Projected area	2.3	m^2
Drag coefficient	1.5	
Terminal velocity	21.8	m/sec

Table 2: Rigid square plate properties

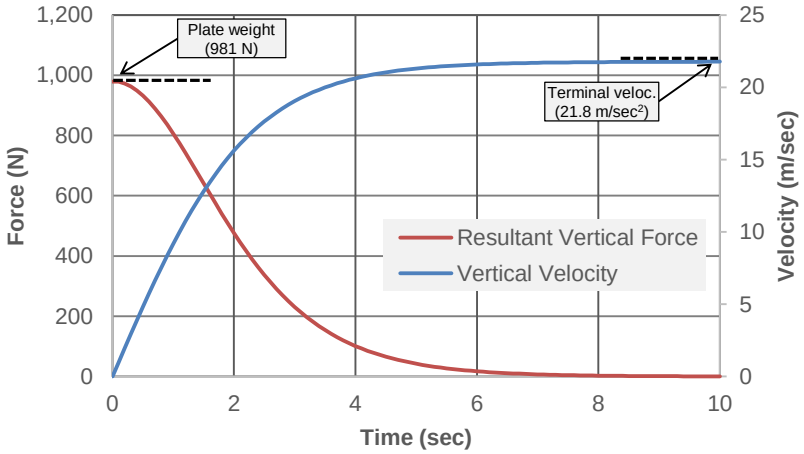

Fig.6: Velocity and resultant force history plot of square plate

4.2 Framed Fabric with Suspended Mass

The purpose of this simulation was to validate the proposed methodology using a basic fabric roof configuration with a highly deformable fabric. The scenario involved a flexible, 0.6-mm thick plate attached to a steel frame. The elastic modulus of the plate was 5 MPa to replicate the compliance of a flexible vinyl fabric. The steel frame was composed of 10 mm diameter steel rods that supported a suspended concentrated mass (Fig. 7). The total mass of this model was 100 kg (fabric, rods, and suspended mass), similar to the mass of the rigid square plate (Table 2). The framed plate has the same

dimensions as the rigid plate of Fig. 5. Therefore, assuming the drag coefficient remains constant even after the change in roof profile due to the applied drag force, the resulting terminal velocity from this simulation should be similar to the calculated terminal velocity of 21.8 m/sec (Table 2). It is noted that the drag forces on the steel frame are neglected.

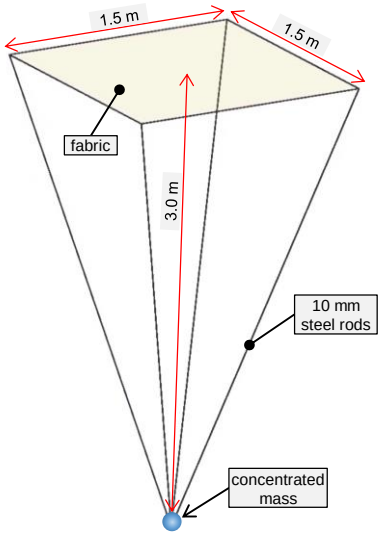

Fig.7: Geometric properties of the framed fabric analysis model

Fig. 8 shows the deformed shape of the framed fabric model in free fall at different times, until it reaches terminal velocity. As the velocity of the model increases due to gravitational acceleration, the roof fabric deforms due to the application of drag forces. However, as can be seen in Fig. 9, the terminal velocity calculated with LS-DYNA is approximately 31 m/sec, which is higher than the theoretical value of 21.8 m/sec. This discrepancy can be attributed to the way the velocity-induced nodal force is calculated. As stated in the implementation section, the velocity component that is used to calculate the applied nodal force is normal to the face of each element. Therefore, as the fabric deforms and becomes curved, the magnitude of the velocity component normal to the surface of the elements adjacent to the edges drops. Because the velocity is lower, the calculated nodal force is also lower. This behavior is illustrated in Fig. 9. The remedy for this condition is to use the resultant nodal velocity at each node to calculate the nodal force. In LS-DYNA this can be achieved by adding extra feedback loops using **`*LOAD_MOTION_NODE`** for the other two components of the nodal velocity.

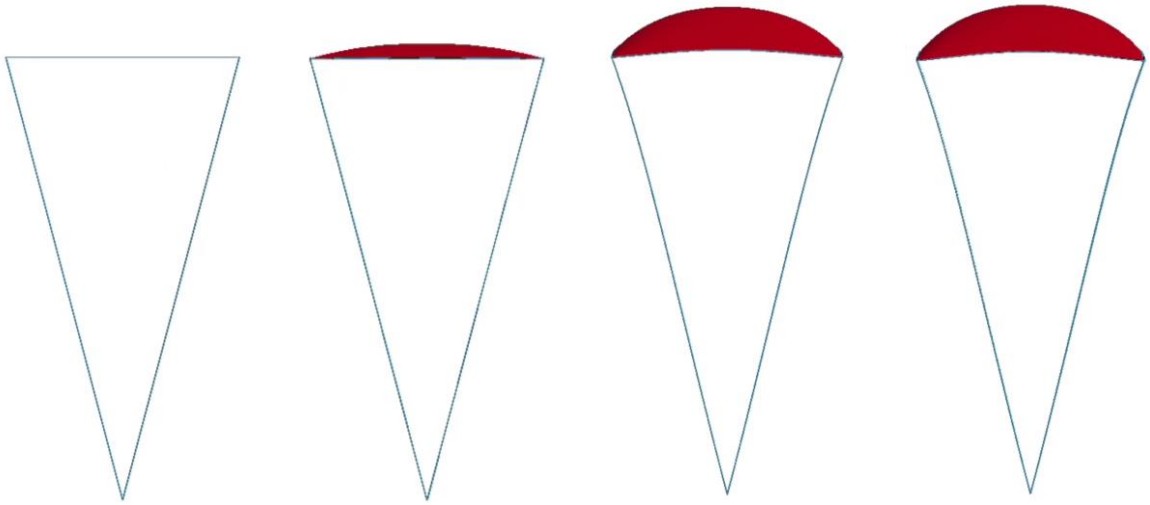

(a) t = 0 *(b) t = 0.4 sec* *(c) t = 4.0 sec* *(d) t = 10 sec*

Fig.8: Deformed shape of framed fabric model in free fall

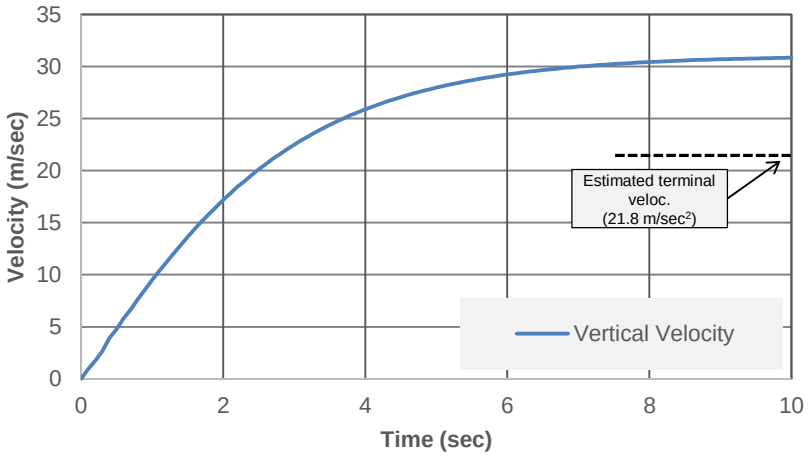

Fig.9: Velocity history plot of framed fabric

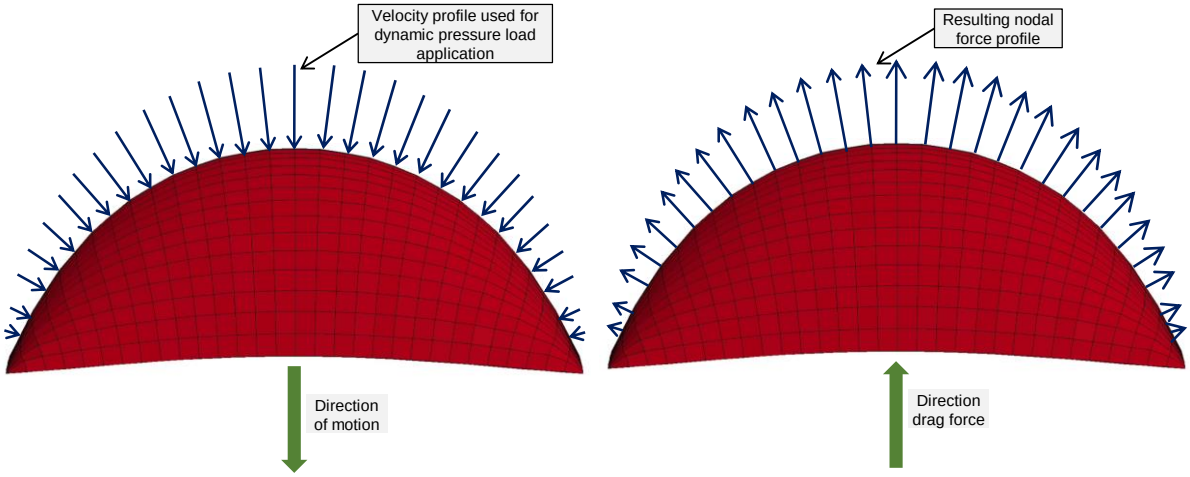

(a) Velocity profile used to calculate nodal forces *(b) Resulting nodal forces*

Fig.10: Velocity and nodal force profile on a curved shape

5 Analysis of a Blast Loaded Fabric Roof

The proposed methodology for drag force was used to evaluate the response of a fabric roof canopy under blast load. The fabric roof canopy provides coverage over an area that is surrounded by sufficiently strong structural walls by which the canopy is supported. The focus of this analysis was the response of the non-tensioned fabric roof cover due to interior detonation at the center of the enclosed area.

5.1 Roof Geometry

The roof canopy is 11.10 m long and 10.20 m wide as indicated in Fig. 11. The supporting framing consists of curved beams that span in the short direction with a 12.00 m curvature radius. The position and spacing of the supporting beams is shown in Fig. 11. The gable ends of the roof canopy are also covered by separate fabric pieces. The fabric roof cover is continuously supported along the gable ends. In the other direction, the fabric is discretely supported by a total of 12 springs (6 at each edge). Each spring is located at the ends of the supporting beams.

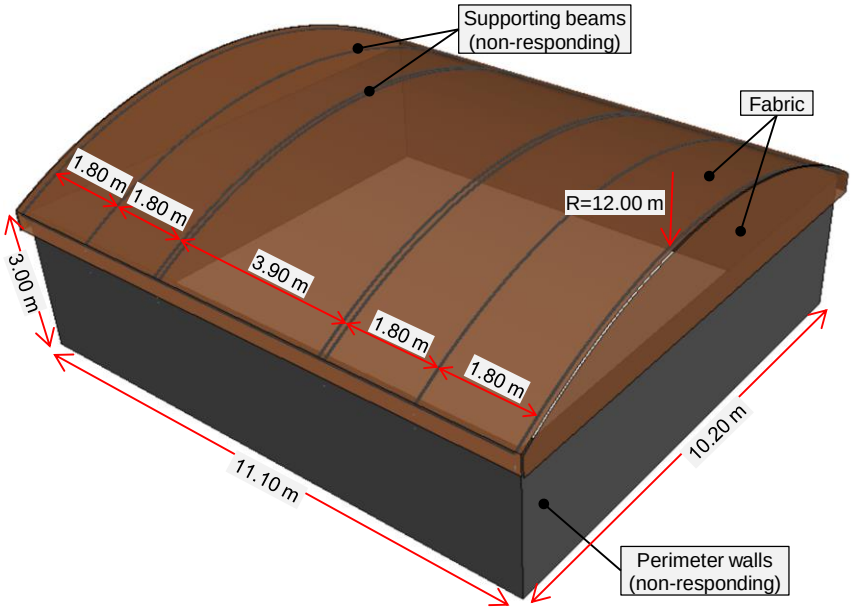

*fabric shown transparent for clarity

Fig.11: Fabric roof canopy analysis model

5.2 Modeling Parameters

The perimeter walls and supporting beams were modeled as rigid (non-responding) members. The fabric cover was representative of a non-breathable, coated vinyl fabric with areal weight of 680 g/m^2. The specified grab tensile strength of the fabric was 750 × 650 N/2.5 cm per ASTM D5034. This fabric was represented in the analysis using the tabulated version of material #34, **`*MAT_FABRIC_MAP`** with 4-noded shell elements (ELFORM=9). The blast load was simulated using **`*LOAD_BLAST_ENHANCED`** for a hemispherical surface burst. The explosive was assumed to detonate at the center of the enclosed area and 4.40 m below the highest point of the roof.

5.3 Response

Following the detonation, the fabric roof expands and has a peak vertical deflection of 1.1 m. The same analysis, without including the effects of drag force, results in peak vertical deflection of 1.9 m. Fig. 12 shows the deflected shape of the roof with and without the effects of drag force during peak vertical deflection. Fig. 13(a) shows the vertical displacement history at the center of the roof. The peak reaction loads at the roof supports are also shown in Fig. 13(b). In the case where drag force was included, the total reaction force was 150 kN, which is considerably lower than the 230 kN reaction force that the analysis without drag force predicted. The appreciable difference between the two analyses demonstrates the overestimation of the roof's response if drag force is not included. In design practice, a more accurate prediction of the roof's response is particularly important as it can lead to a more economical fabric and support structure design.

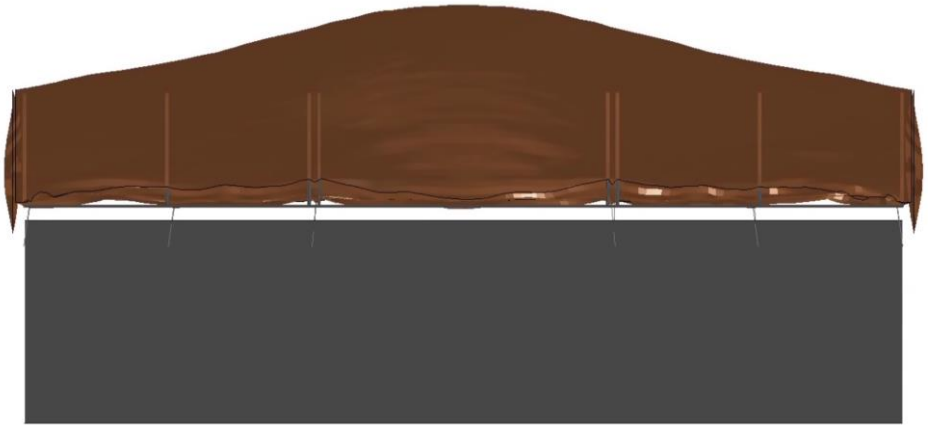

(a) Analysis with drag force, t = 78 msec (peak displacement: 1.1 m)

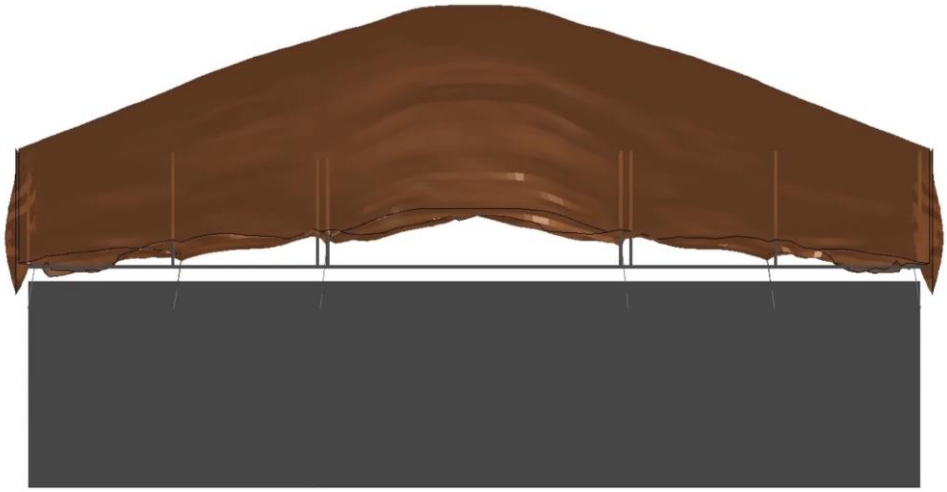

(b) Analysis without drag force, t = 64 msec (peak displacement: 1.9 m)

**fabric shown transparent for clarity*

Fig.12: Side view of roof response during peak vertical displacement

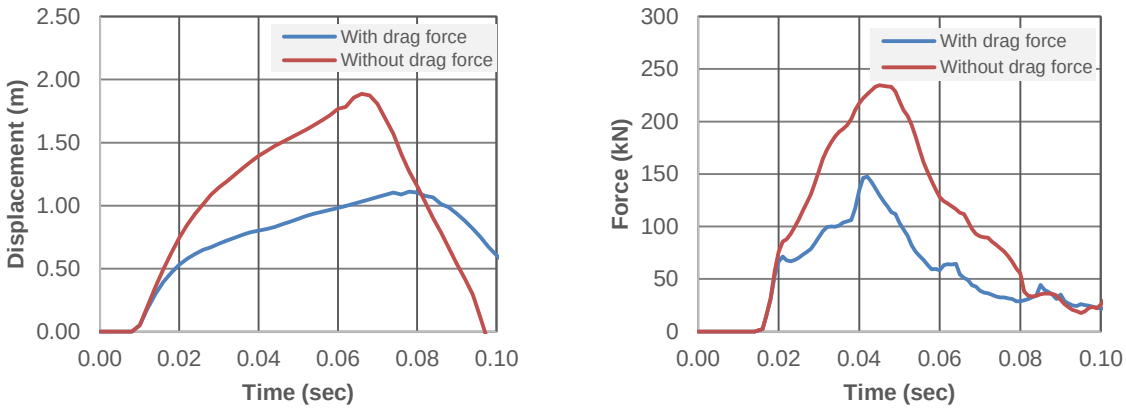

(a) Vertical velocity at middle of roof *(b) Vertical reaction force at supports*

Fig.13: Response of fabric roof in blast with and without including drag force

6 Summary

This paper presents a simplified approach to include the effects of fluid resistance due to the dynamic motion of an object inside a fluid domain. The proposed methodology can be implemented in LS-DYNA using standard keywords and without the need to employ a coupled CFD modeling approach. Due to its

simplicity, the modeling approach presented herein possesses a number of inherit limitations related to accurate representation of the pressure gradient at the exposed surface of an object. Nonetheless, it can capture with reasonable accuracy the velocity-dependent fluid pressures acting on a moving object. This makes it suitable for design-level analyses where the variation of drag force is of main interest. The validity of this approach has been presented with a number of validation analyses. A useful application of the proposed methodology is the dynamic response prediction of flexible, lightweight structures under blast loads. In this scenario, the blast-loaded structure is expected to experience relatively large-amplitude dynamic motion, which generates appreciable dynamic pressure resistance. A relevant example was presented herein, which demonstrated how influential drag force resistance can be to the overall motion of a blast-loaded fabric roof canopy.

7 Literature

[1] “fabric-roof-structure - Ceno Tensile Structures.” [Online]. Available: https://www.sattler-global.com/textile-architecture/fabric-roof-structure-1482.jsp. [Accessed: 04-Apr-2019].

[2] “New Fabric Cover to QRA Shelters 1,2,3 - AWD Contractors.” [Online]. Available: http://www.awdcontractors.ca/index.cfm/gallery/britespan-buildings/new-fabric-cover-to-qra-shelters-1-2-3/. [Accessed: 04-Apr-2019].

[3] B. Tutt, S. Roland, R. Charles, and G. Noetscher, “Development of Parachute Simulation Techniques in LS-DYNA®,” p. 12.

[4] T. Rose, G. Noetscher, and K. Bergeron, “Simulation and Testing Assessment of Cruciform Parachutes using LS-DYNA® ALE,” p. 8, 2018.

[5] G. J. Vassilakos, “Elemental Water Impact Test: Phase 1 20-inch Hemisphere,” p. 60.

[6] B. Perin, O. Verdrel, P. Bordenave, E. Grippon, V. Lapoujade, and H. Belloc, “Computational Fluid Dynamic of NACA0012 with LS-DYNA® (ALE & ICFD) and Wind Tunnel Tests,” 2016, p. 12.

[7] G. Laird, K. Fraser, and R. Marsh, “Interactive Dynamic Analysis of Subsea Lifting Ropes,” 2016, p. 17.

[8] L. J. Clancy, *Aerodynamics*. Wiley, 1975.

[9] “Minimum Design Loads and Associated Criteria for Buildings and Other Structures (7-16).” [Online]. Available: https://sp360.asce.org/PersonifyEbusiness/Merchandise/Product-Details/productId/233133882?_ga=2.183393958.1858516032.1554735167-1512663864.1541514831. [Accessed: 08-Apr-2019].

[10] “Drag Fluids.” [Online]. Available: http://www.roymech.co.uk/Related/Fluids/Fluids_Drag.html. [Accessed: 09-Apr-2019].